Delft University of Technology

SC42065

Closed Loop Control using Classical Adaptive Optics

Authors

Laura Maddalena (908007)

Leonoor Tideman (4298322)

Paulo Cerqueira (4710444)

Pranav Prakash (4709373)

Satyajith Jujjavarapu (4708547)

July 26, 2018

1 Introduction

The aim of this work is implementing a classical adaptive optics system for correcting the wavefront aberrations. The system was implemented following the approach used in astronomy. An aberrated coherent light source is used to mimic the the light coming from a star. The wavefront distortion is detected using a Shack-Hartmann (SH) wavefront sensor. Subsequently, a controller for correcting aberrations using a bimorph piezoelectric deformable mirror (DM) was developed. The aberration can be either static (varies spatially) or dynamic (varies spatio-temporally).
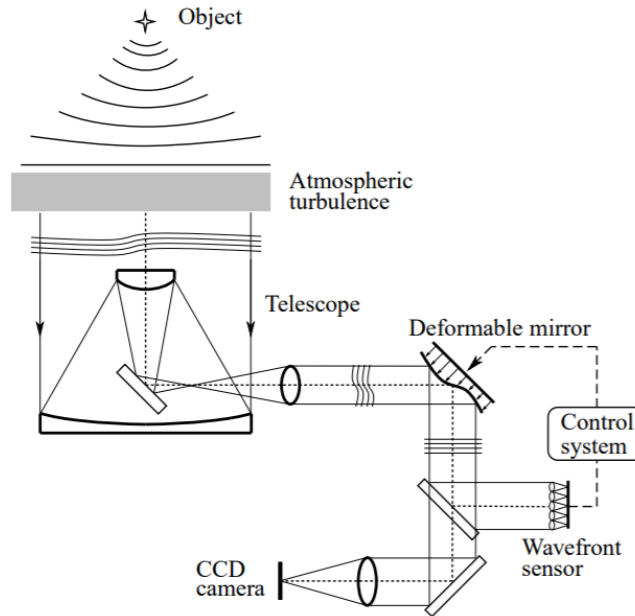

Figure 1: A sketch of the classical adaptive optics setup [1]

2 Set-up description

The main components used in the optical setup are shown in Figure 2. A coherent light source of wavelength 635 nm emitted by a diode laser is collimated using the lenses *L1* and *L2*, each of focal length $50mm$. Aberration are produced at the iris i plane using a transparent material coated with hair spray (or gel) to introduce an index of refraction mismatch. The aberration plane has to be conjugated with the *DM* plane and the *SH* plane. Conjugation is achieved by using two Keplerian telescopes. The first telescope was built using lenses *L3* and *L4* each of focal lengths 50 mm and 300 mm respectively. This telescope requires considerable magnification ($M = 6$) because we aim to sample the wavefront distortions with the DM actuators. On the other hand, the second telescope with lenses *L5* and *L6* of focal lengths 200 mm and 60 mm respectively, demagnifies ($M = 0.3$) the beam to fill the SH sensor. The lens *L7* focuses the beam onto the CMOS camera for imaging. The distance between the lens and beam splitter was determined such that the whole beam would be captured on the camera sensor, despite possible divergences due to aberrations.

In order to align the system, base voltages (Secion3) were applied to the 40 actuators of the DM. We manually verified that the light beam is collimated (parallel with constant diameter). The DM's defocus was tuned to make sure that the SH sensor was properly placed and could measure the whole Shack-Hartmann pattern (without cutting off the peripheral spots). Once the sensor was successfully aligned in the conjugate plane of the aberrations, the DM's defocus was set back to zero.
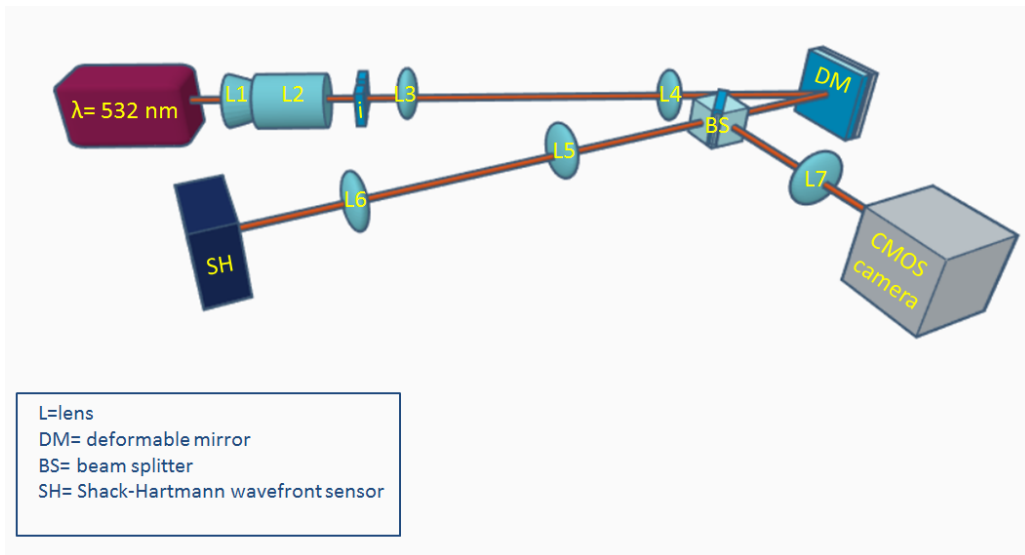
Figure 2: Sketch of the adaptive optics setup

3 Calibration of the system

3.1 Centers of the Shack-Hartmann pattern

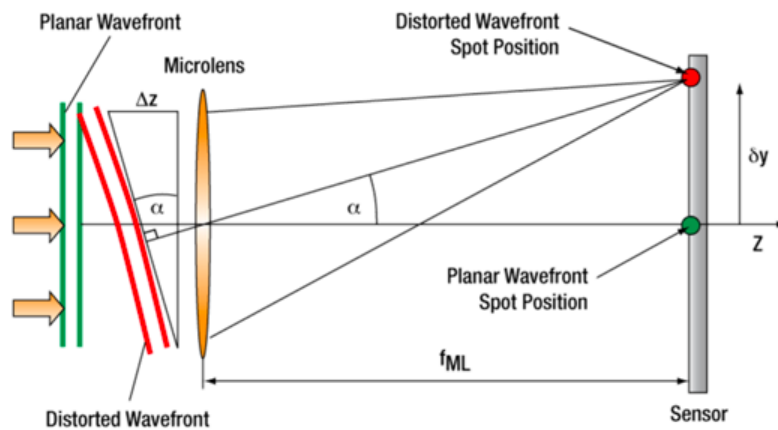A SH sensor consists of a microlens array coupled to a CMOS camera as illustrated in Figure 3.

Figure 3: Sketch of the adaptive optics setup [2]

The local slope of wavefront $\phi(x, y)$ across each microlens is derived from the focal spot's displacement on the sensor as described in Equation 3.1 where f_{ml} is the microlens array focal length, δx and δy are the spot displacement from the reference.

$$\frac{\partial \Phi(x, y)}{\partial x} = \frac{\delta x}{f_{ml}} \qquad \frac{\partial \Phi(x, y)}{\partial y} = \frac{\delta y}{f_{ml}} \tag{3.1}$$

In order to measure the wavefront slopes, the SH sensor must be able to determine deviations of the spots from a flat wavefront taken as reference. Hence the importance of accurately identifying the SH reference spots.

We start by thresholding the image, and then looking for which pixels have the highest value. Once these maximum pixels have been located, we black out the surrounding square of 25x25 pixels and proceed identically by looking for the highest pixel values in the rest of the image. The search for high value pixels continues until the maximum reaches a threshold of 20. As a result, each spot in the SH pattern is assigned a box, and the centers-of-mass of these boxes will be the reference when computing the focus spot displacements. The same boxes are also used to compute the centers-of-mass in the aberrated scenarios, under the assumption that each aberrated spot remains within the box of its corresponding reference spot.

The position of each n$^{\text{th}}$ center-of-mass in the image (x_n, y_n) (based on the center of mass weighed by illumination) was computed using the following formulas, where u and v are the absolute coordinates of the pixels in the image and $I(u, v)$ is their corresponding brightness on a greyscale from 0 (black) to 255 (white).

$$x_n = \frac{\sum_{u,v} u \cdot I(u, v)}{\sum_{u,v} I(u, v)} \qquad y_n = \frac{\sum_{u,v} v \cdot I(u, v)}{\sum_{u,v} I(u, v)} \tag{3.2}$$

3.2 Optimization of the mirror actuators' base voltages

It is important to re-calibrate our Adaptive Optics system before every use to account for hysteresis of the piezoelectric actuators of the DM. Before being able to correct aberrations, we must ensure it performs well in their absence. The base voltages are the optimal DM actuator voltages that result in a good point spread function (PSF) when the incoming wavefront is perfectly flat. We start by thresholding the image to remove background noise, then we identify the image's center of mass coordinates $u^{\star}$ and $v^{\star}$ (weighed by illumination) and compute their second moment:

$$I = \frac{\sum_{u,v} I(u, v) \cdot ((u - u^{\star})^2 + (v - v^{\star})^2)}{\sum_{u,v} I(u, v)} \tag{3.3}$$

Optimization is performed as follows: one of the DM's actuators is (randomly) selected at a time. The voltage of this selected actuator is (randomly) increased or decreased by less than 5V. The second moment is calculated as per Equation 3.3 and compared to the second moment of the previous voltage distribution. If the new second moment is inferior to the previous image's second moment, the voltage increment on that specific actuator is considered successful and retained: the updated optimal voltage distribution will include this local increment. Otherwise, the actuator voltages are set to their previous values and we try once again to improve the optimal voltage distribution by poking another actuator with a different voltage increment, so that the second moment of the image decreases.

Figure 4 shows that the optimization of the base voltages of the DM successfully improves the PSF obtained by the camera without aberrations.
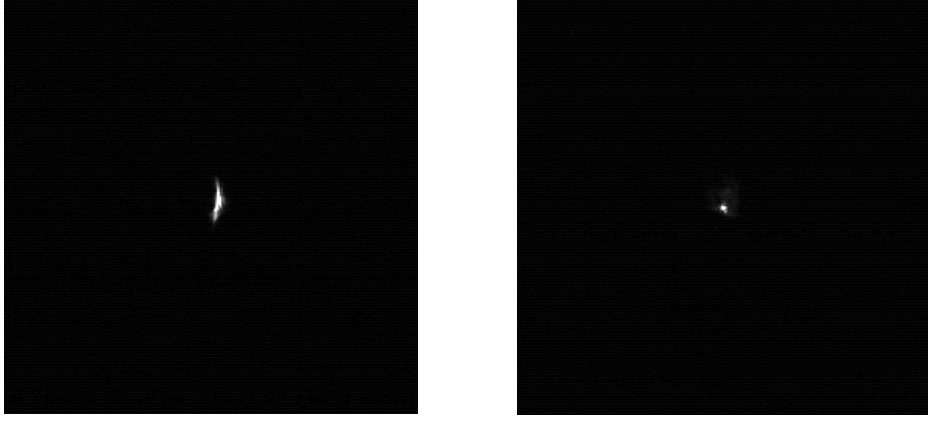
Figure 4: Pre-optimization PSF (left) and post-optimization PSF (right), with increased brightness

4 Determining the mirror's control matrix H

The control inputs are selected by solving a least-squares problem (Section 5) that requires knowledge of the mirror's control matrix H. Matrix H relates the input voltages to the center-of-mass displacements caused by shape of the DM as follows:

$$y_{\mathrm{DM}} = Hu$$

In the absence of aberrations, the residual wavefront $\varepsilon = \phi + \phi_{\mathrm{DM}}$ simplifies to $\varepsilon = \phi_{\mathrm{DM}}$. The mirror's control matrix is obtained by measuring the center-of-mass deviations resulting from the individual prompting of each mirror actuator, a method called "poking the mirror". By applying voltage V to one actuator at a time, each of the 40 columns of H, denoted H_i with $i \in \{1, 2, \ldots, 40\}$, is related to the measured center-of-mass deviations y_i as per Equation 4.1.

$$u_1 = \begin{pmatrix} V \\ 0 \\ 0 \\ \vdots \end{pmatrix} \implies y_1 = V \cdot H_1 \iff H_1 = \frac{y_1}{V}$$

$$u_2 = \begin{pmatrix} 0 \\ V \\ 0 \\ \vdots \end{pmatrix} \implies y_2 = V \cdot H_2 \iff H_2 = \frac{y_2}{V} \tag{4.1}$$

$$\vdots$$

$$u_{40} = \begin{pmatrix} 0 \\ 0 \\ \vdots \\ V \end{pmatrix} \implies y_{40} = V \cdot H_{40} \iff H_{40} = \frac{y_{40}}{V}$$

The voltages were set to be $V = 50$ V so as to sufficiently deform the mirror and obtain relevant center-of-mass deviations y_i. In practice, this approach will not yield perfect results due to noisy measurements and possible non-linearities, which have implications in control (refer to Section 5).

5 Controller design

The control input u was designed by disregarding the temporal dimension, and focusing on the spatial dimensions. This makes the controller well-suited for correction of static aberrations, yet less so for

dynamic aberrations. In fact, when attempting to correct dynamic aberrations, the controller is only expected to improve the image when the aberration does not vary significantly between consecutive time-steps.

To better grasp the problem, a static aberration ϕ is considered (as the control design ignores time), and the matrix that relates the control input to the phase ϕ_{DM} of the deformable mirror is denoted $\mathcal{H}$, to distinguish it from H, which relates the input to the SH pattern center-of-mass displacements. The residual wavefront, at time-step k, is given by Equation 5.1.

$$\varepsilon_k = \phi + \mathcal{H}u_{k-1} \tag{5.1}$$

Correction can then be tackled by shaping the deformable mirror so as to eliminate the center-of-mass displacements seen in the SH sensor, only considering spatial correction. Application of the input u_k may yield a fitting error ξ_k due to the non-invertibility of $\mathcal{H}$, and the following problem arises:

$$\phi + \mathcal{H}u_k = \xi_k \tag{5.2}$$

Since the SH sensor does not detect ϕ, but the residual wavefront ε_k instead, defining $u_k = u_{k-1} + \delta u_k$, Equation 5.2 should be combined with Equation 5.1 to yield:

$$\phi + \mathcal{H}u_k = \xi_k$$
$$\Rightarrow \phi + \mathcal{H}u_{k-1} + \mathcal{H}\delta u_k = \xi_k$$
$$\Rightarrow \varepsilon_k + \mathcal{H}\delta u_k = \xi_k$$

This is a least-squares problem to solve for the δu_k that minimizes the fitting error ξ_k. In terms of center-of-mass displacements (so as to use the available matrix H, instead of $\mathcal{H}$), the solution is given by the pseudo-inverse $H^\dagger$ of H:

$$\boxed{\delta u_k = -H^\dagger y_k}$$

with y_k being the measured center-of-mass (intensity) displacements seen by the SH sensor. Note that the obtained solution is for δu_k and not u_k itself. Indeed, if major corrections were done in previous time-steps, recomputing the whole u based on the current measured error would revert those corrections. Instead, δu_k is computed and added to the previous corrections.

As mentioned in the previous section, it is to be expected that the computation of H is imperfect, with some actuators modeled worse than others. The actuators may also saturate. This lack of confidence in H may warrant application of a gain $K < 1$, resulting in the control input:

$$\boxed{\delta u_k = -KH^\dagger y_k} \Rightarrow \boxed{u_k = u_{k-1} - KH^\dagger y_k}$$

6   Using SVD to remove the influence of the noisy modes

We consider the singular-value decomposition of the deformable mirror's control matrix: $H = USV^T$ where the columns of U are the left-singular vectors, the diagonal entries of S are the singular values of H, and the rows of V are its right-singular vectors. The SVD is computed as follows: for $i = \{1, 2, \ldots, 40\}$, the left-singular vectors u_i are the eigenvectors of HH^T, the right-singular vectors v_i are the eigenvectors of $H^T H$ and the singular values σ_i are the square-roots of the eigenvalues of both HH^T and $H^T H$. The pseudo-inverse of H is given by Equation 6.1. The pseudo-inverse of S is formed by replacing every non-zero diagonal entry by its reciprocal and transposing the resulting matrix.

$$H = USV^T \Rightarrow H^\dagger = VS^\dagger U^T \tag{6.1}$$

The advantage of computing the pseudo-inverse of H using the SVD method is that we can consider a truncated matrix $\tilde{H}$ whose modes corresponding to the smallest, possibly noisy, singular values have been removed. We have $\tilde{H} = U\tilde{S}V^T$ where the rank of $\tilde{S}$ is equal to the number of modes considered.

The spacing between consecutive singular values and their relative sizes indicate after which dominant modes to truncate, and which possibly noisy modes to leave out. However, the noisy modes may be hard to distinguish from modes that contain meaningful information, which is why the truncation of H may reduce the quality of reconstruction and control. The singular values of H are shown in Figure 5
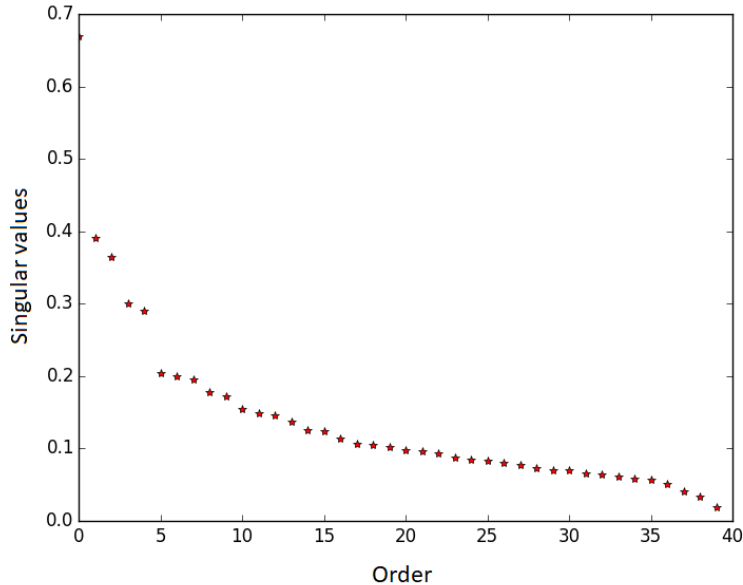

Figure 5: Singular values of H

6.1 Voltage reconstruction

In the absence of external aberrations, the measurement of the center-of-mass displacements of the SH pattern, through use of H, should allow recovery of whichever voltages are applied to the mirror actuators. Imperfections in H will thus lead to erroneous reconstruction of the applied voltages. To test the quality of the obtained H and its inverse, taken with different amounts of modes, each actuator was subjected to voltage offsets ranging from -60 V to 60 V in steps of 20 V, and reconstruction of these was attempted from measurements of the SH pattern displacements. For each of the 40 actuators, the reconstructed voltages were plotted as a function of the applied voltages, which, in the case of perfect modelling of the actuator, should yield a line at $45°$. Flat or nonlinear curves show imperfect modelling.

The results of voltage reconstruction with the pseudo-inverse $H^\dagger$ of the DM's control matrix H are presented in Figure 6. When considering all 40 modes of the system, the reconstructions of most actuators display a slope of approximately $45°$ which means that the real voltage is equal to the reconstructed voltage, although some actuators display significant biases. Figure 7 shows that the reconstruction of the voltages of certain actuators is deteriorated by the removal of the two lowest modes, with these curves being flatter than the ones obtained with 40 modes. However, with all 40 modes, the reconstructed voltages of several actuators showed large biases, which were reduced when the two smallest modes were removed. Nonetheless, overall, reconstruction of the voltages with 40 modes was better. Despite the two removed smallest modes being associated to noise, the truncated pseudo-inverse $\tilde{H}^\dagger$ is less accurate than $H^\dagger$, resulting in several actuators having flawed voltage reconstructions.

In the sections that follow, each of the 40 actuators is labelled with a number. Figures 6, 7, and 8 display these actuators by order, from left to right, then top to bottom.
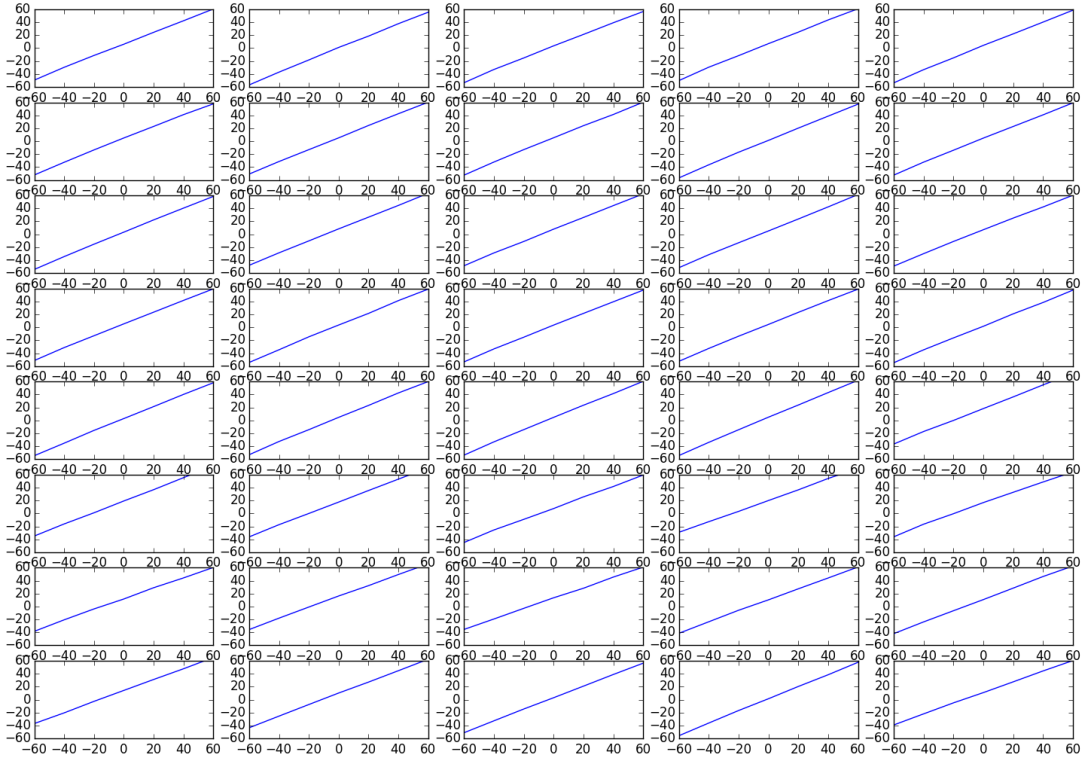
Figure 6: Voltage reconstruction with $H^\dagger$ considering all 40 modes
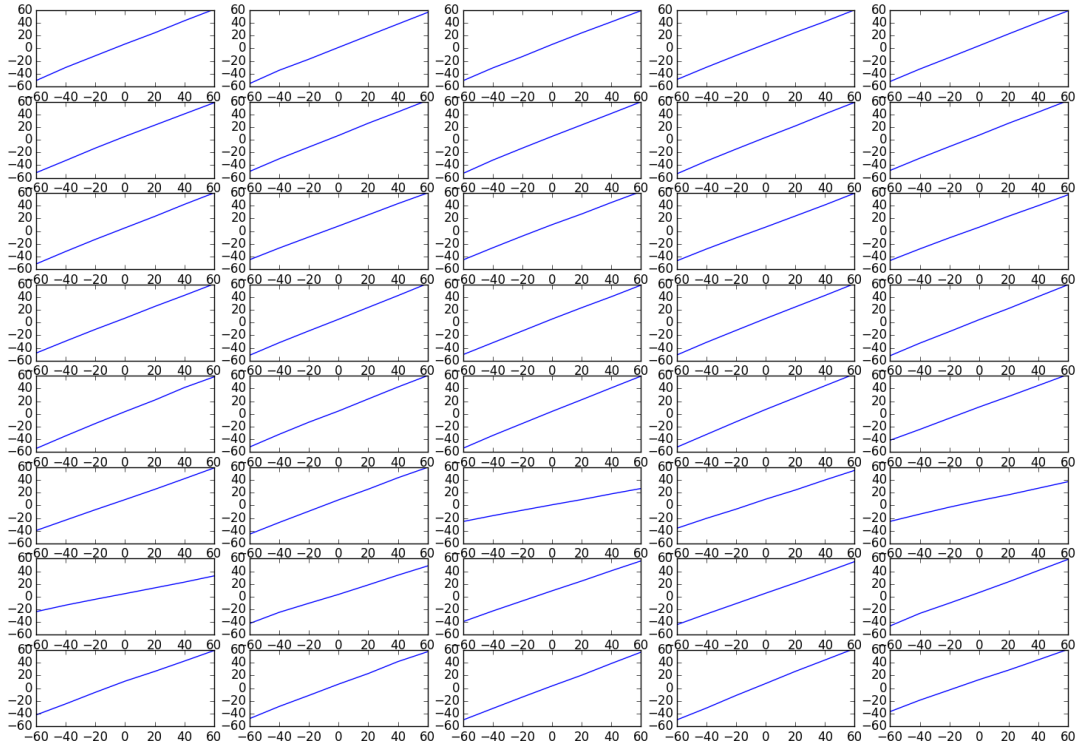

Figure 7: Voltage reconstruction with $\tilde{H}^\dagger$ considering 38 modes

Figure 8 demonstrates how the voltage reconstruction is further deteriorated when only the five highest modes are retained in the computation of $\tilde{H}^\dagger$. All of the deformable mirror's actuators present almost horizontal reconstruction slopes. Contrarily to the voltage reconstruction in Figure 6, that of Figure 8 fails.
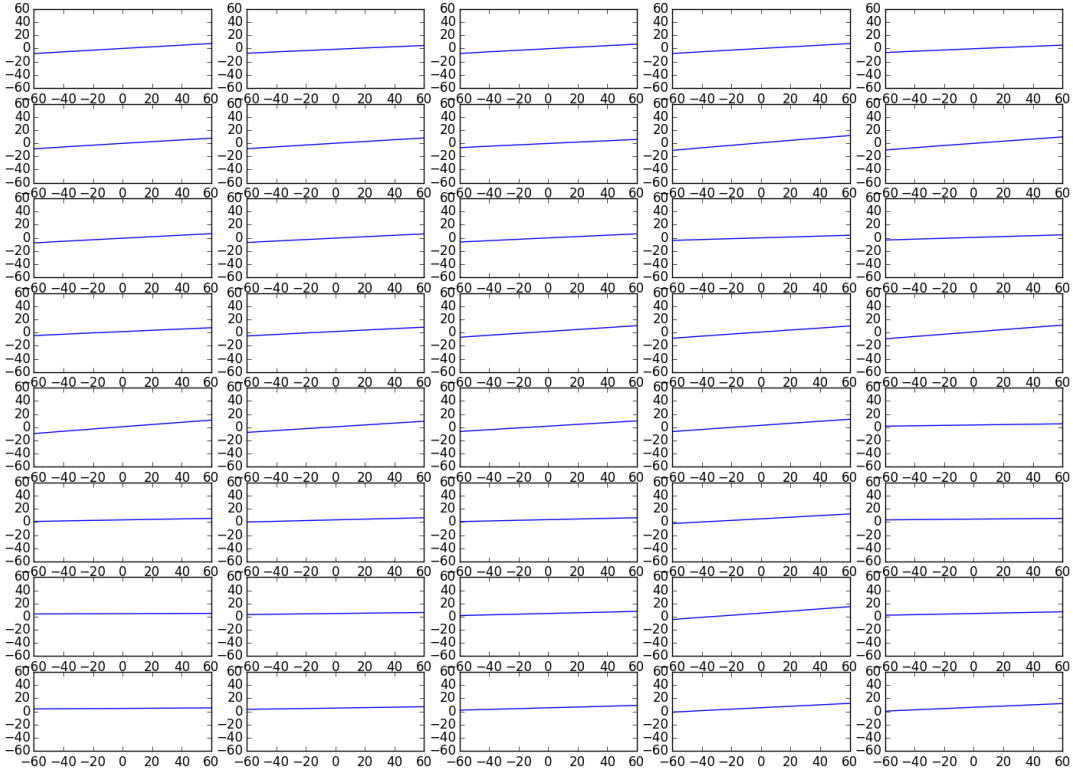
7

Figure 8: Voltage reconstruction with $\tilde{H}^\dagger$ considering only 5 modes

7 Voltage correction

Ideally, the mirror control matrix H would be invertible and accurately measured. In the absence of aberrations, if the initial voltages of the mirror were set to random values and a controller with gain $K = 1$ was then put to action, the voltages would converge to zero in a single step. Lower controller gains would result in slower convergence.

However, neither is H perfectly captured, nor is it invertible: there are only 40 actuators for over 670 spots in the Shack-Hartmann pattern. The performance of the designed controller, put to the test with gain $K = 0.5$ in the aforementioned scenario, is shown in this section for different numbers of modes. The initial voltages were set to random values with a maximum deviation of 50 V from the base voltages.

Voltage correction with 40 modes (pseudoinverse)

The result of the correction of random voltages with the pseudoinverse of H is presented in Figure 9:
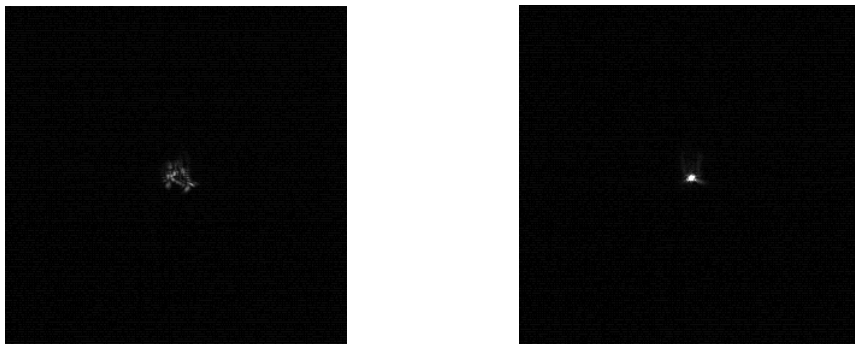
Figure 9: Initial aberration due to random voltages applied to the mirror (left) and corrected image using all 40 modes of H (right)

The vector of final voltage deviations from the base voltages had a norm of 99.74 V, with the following deviations per actuator:
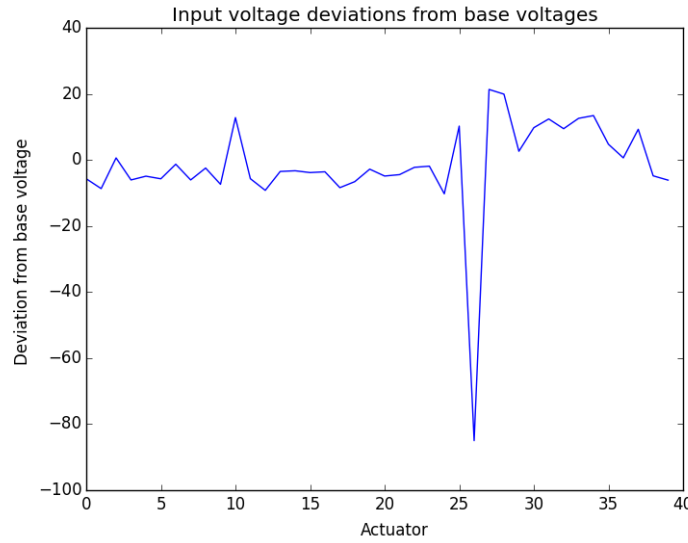

Figure 10: Excess voltages over the base voltages applied to each actuator when correcting with 40 modes of H

The controller satisfactorily corrected the aberration created by the random initial voltages, yet not by reducing its deviation from the base voltages to zero. Instead, due to the imperfect reconstruction and the improper modelling of some of the actuators, it found another solution, effectively correcting the aberration, but not by reducing its deviation from the base voltages to zero (refer to Subsection 3.2 for the meaning of "base voltages"). One of the actuators, the 26th, was especially badly modelled, displaying a large deviation from the base voltages at the end of the correction. Looking at Figure 6, it is visible that this actuator was modelled with a large bias.

Voltage correction with 38 modes

As explained in Section 6, the controller was tested after having removed probable noisy modes in order to improve reconstruction. Removal of the smallest two singular values led to the following results:
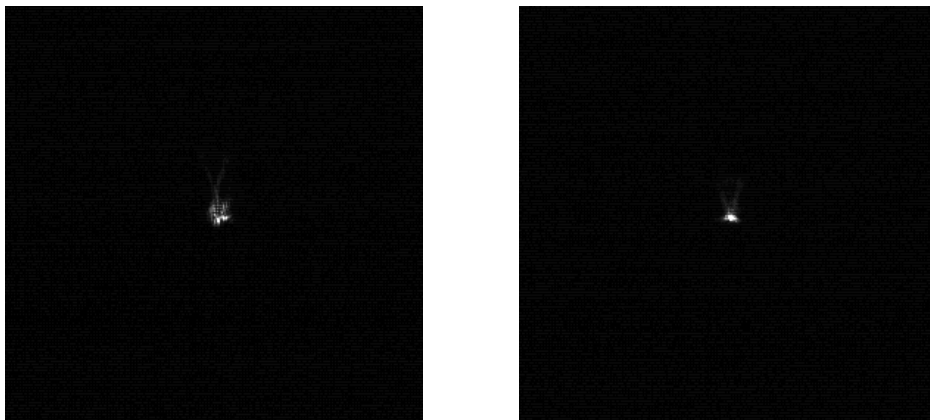

Figure 11: Initial aberration due to random voltages applied to the mirror (left) and corrected image (right) using 38 modes of H

The vector of final voltage deviations has norm 129.07 V. The voltage deviation per actuator is shown below:
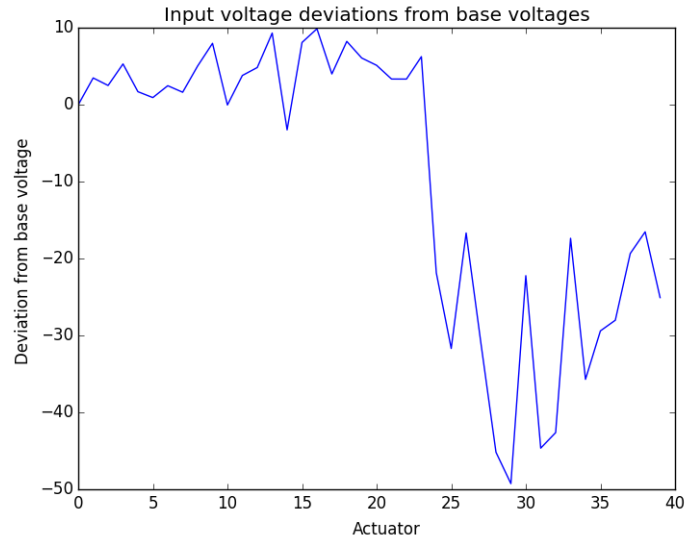
9

Figure 12: Excess voltages over the base voltages applied to each actuator when correcting with 38 modes of H

Although the wavefront aberrations were successfully corrected, Figure 12 demonstrates that the removal of the last two modes caused significant loss of information. Indeed, half the actuators are poorly modelled since their voltage deviations do not tend to zero. This suggests that removing more modes will lead to further deterioration of the quality of the results. In order to ascertain this hypothesis, we nevertheless measure the actuator voltages after removing 5 and 35 modes.

Voltage correction with 35 modes

Consideration of only the first 35 modes of H when calculating its pseudo-inverse led to the results presented in Figure 13.
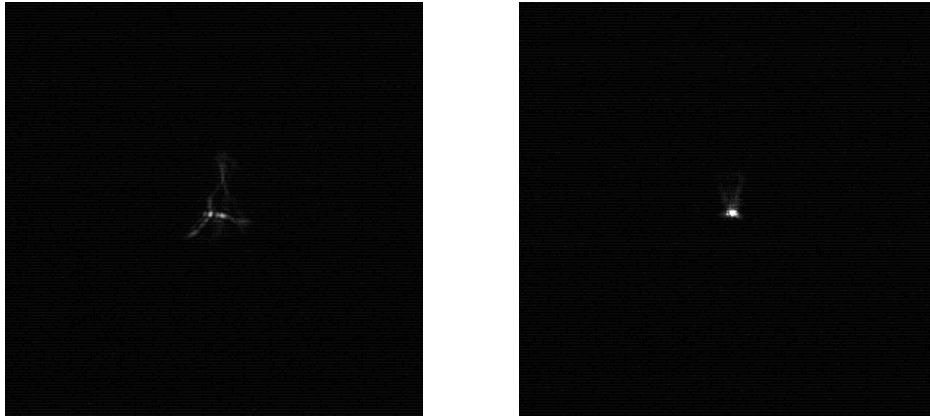
Figure 13: Initial aberration due to random voltages applied to the mirror (left) and corrected image (right) using 35 modes of H

The final voltage deviation vector has a norm of 102.67 V, and the voltage deviation per actuator is shown hereunder:
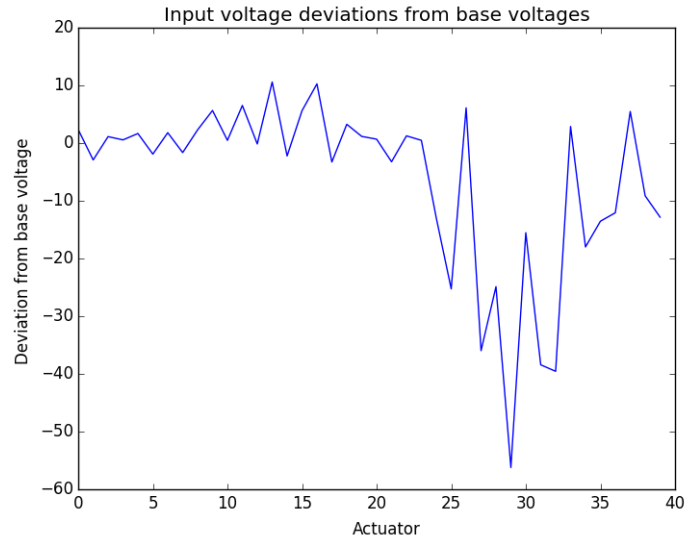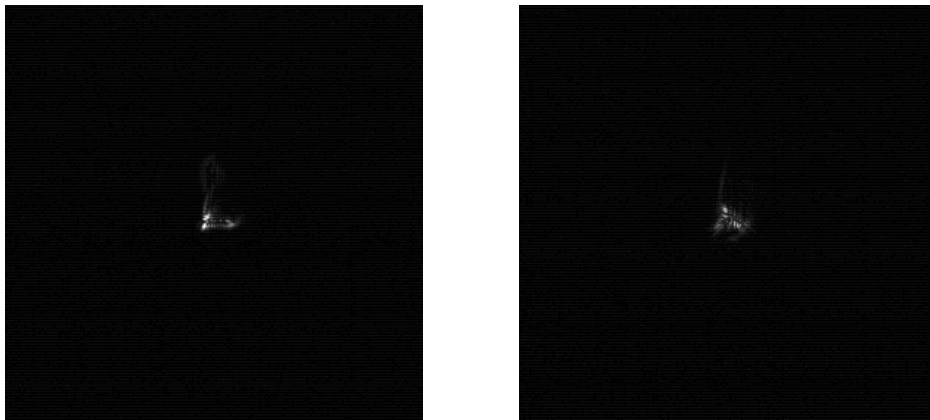
Figure 14: Excess voltages over the base voltages applied to each actuator when correcting with 35 modes of H

Correction of the aberration was successful. The voltage applied to some of the actuators was reduced with respect to the correction with 38 modes, whereas others saw an increase, making it hard to observe any improvement or deterioration. The modelling of the actuators, however, appears to remain worse than that done with all 40 modes.

Voltage correction with 5 modes

Resorting only to the first five modes of H, another correction was attempted. Indeed, there is a large gap between the fifth and sixth singular values, as visible in Figure 5, suggesting a possible trimming point. As expected, this results in a significant loss of information. The results are shown in Figure 15.

Figure 15: Initial aberration due to random voltages applied to the mirror (left) and corrected image (right) using 5 modes of H

The first five modes were not enough for correction of the aberration caused by the mirror itself. The deviations from the base voltages had a norm of 268.36 V, and are shown in Figure 16.
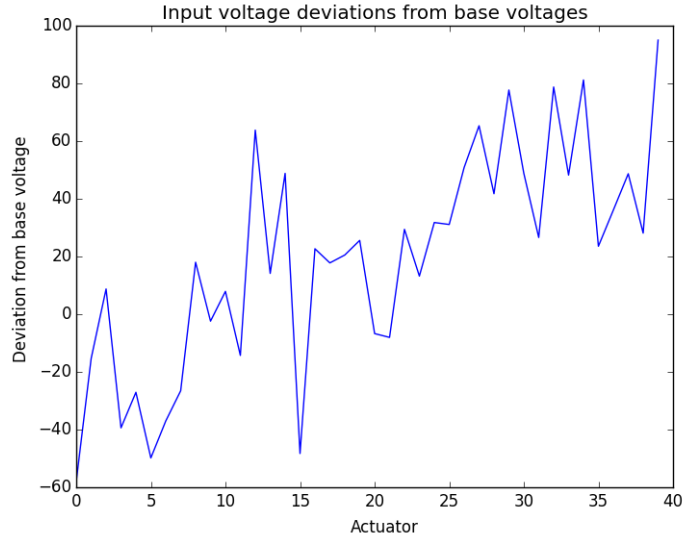
Figure 16: Excess voltages over the base voltages applied to each actuator when correcting with 5 modes of H

The final voltage deviations seem random: five modes are clearly not enough to adequately model the mirror dynamics.

8 Static aberrations

The controller is expected to adequately correct static aberrations. As motivated in Section 6, the removal of noisy modes from the singular-value decomposition by truncating it at the first m modes, for an adequately chosen m, may improve the performance of the controller. As such, results for different amounts of modes will be presented, with $m \in \{5, 10, 15, 20, 25, 30, 35, 36, 37, 38, 39, 40\}$ modes, with 40 modes corresponding to the original deformable mirror control matrix H. The gain was set to $K = 0.5$.

Five different aberrations were corrected for each number m of modes. The quality of the correction was assessed by measuring the variances of the Shack-Hartmann pattern deviations. The mean variances of all five aberrations for the last 50 frames (out of a total of 100 frames) are compared in Figure 17. Aberration nº1 has the lowest mean variance, regardless of the number of modes used to invert the deformable mirror's control matrix: this suggests the aberration was too small. Observing Figure 17 suggests the correction of aberration nº4 is the worst since the mean variance is largest. The correction of aberration nº3 seems to be better than that of aberrations nº2 and nº5. However, rigorously evaluating the quality of these aberration corrections requires knowledge not only of the mean variance, but also of the variance of the 50 frames' variances. Indeed, the better the performance, the smaller the variance of correction variances should be.
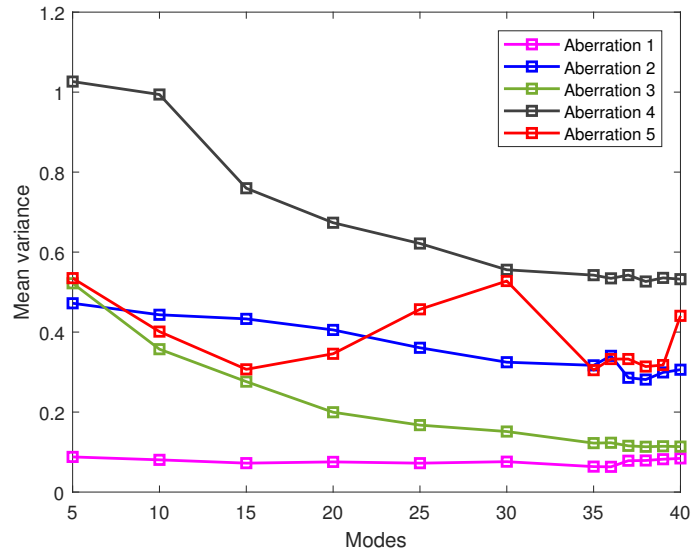
12

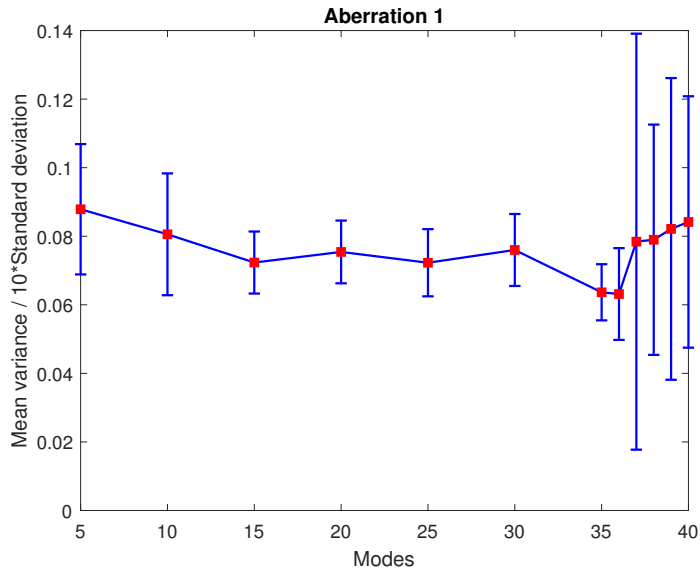Figure 17: Mean variance of all five aberrations

Figure 18: Mean variance and scaled standard deviation of the variances of aberration 1

Figures 19, 20, 21 and 22 hereafter show the mean variance of aberration corrections, as well as the standard deviation of the 50 frames' variances. As indicated in the y-axis of the Figures, the standard deviation was increased by a factor 10 to facilitate the comparison.
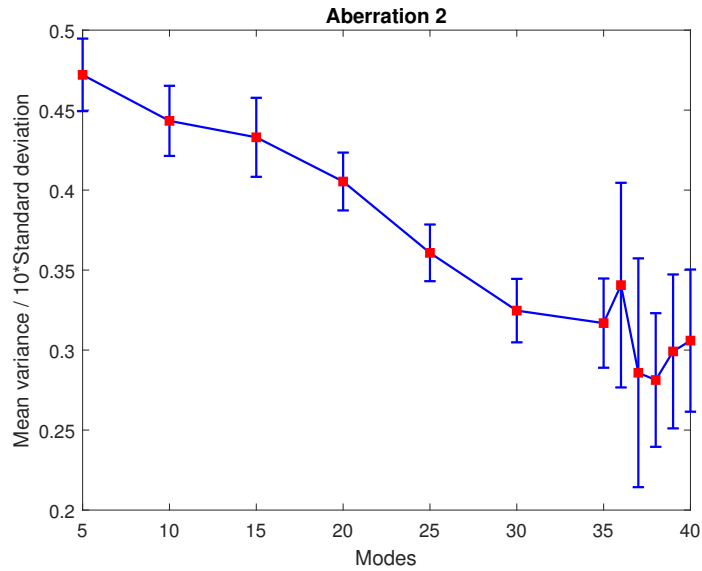
Figure 19: Mean variance and scaled standard deviation of the variances of aberration 2

According to Figure 19, the best correction of aberration n°2 corresponds to mode 38 where the mean variance is 0.28 and the standard deviation of the mean is 0.0042. Figure 19 demonstrates that the correction of aberration n°3 has a very small standard deviation. From modes 35 to 40, the correction of aberration n°3 is excellent: the mean variance is around 0.116, and the standard deviation is around 0.0012.
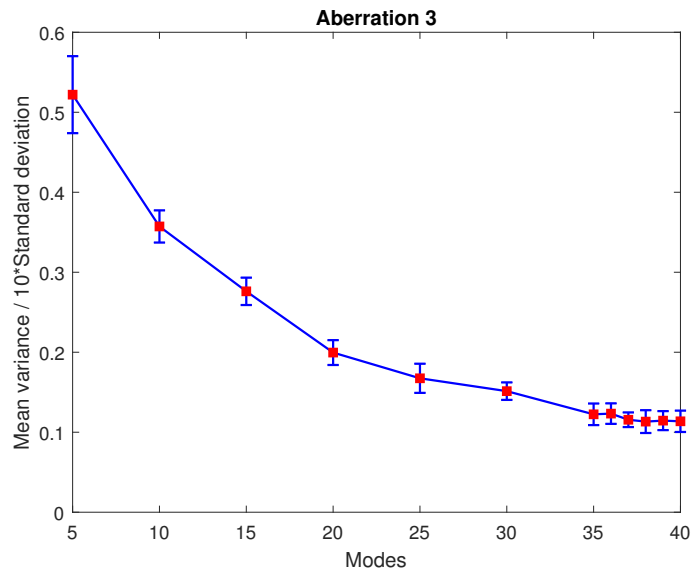

Figure 20: Mean variance and scaled standard deviation of the variances of aberration 3

Figure 21 confirms that the correction of aberration n°4 is the worst: not only is the mean variance high (approx. 0.66), the standard deviation is also very high (approx. 0.05). Finally, aberration n°5 shows a relatively stable standard deviation (approx. 0.0031) despite rather large variations of the mean variance. Both aberrations n°4 and n°5 are best corrected when 35 or 38 modes are considered (minimum mean and minimum deviation).
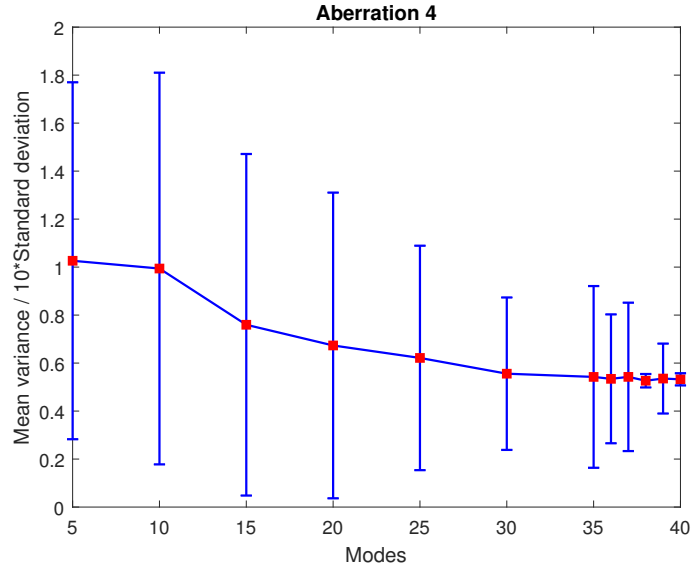
14

Figure 21: Mean variance and scaled standard deviation of the variances of aberration 4

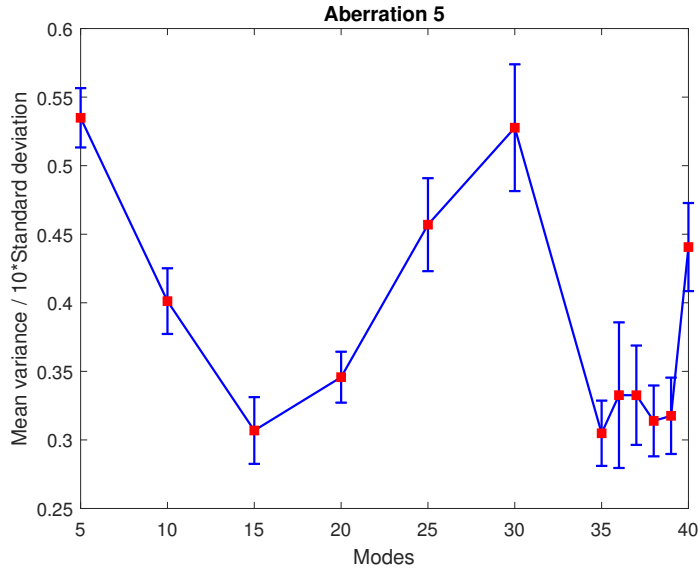Figure 22: Mean variance and scaled standard deviation of the variances of aberration 5

9 Dynamic aberrations

Certain dynamic aberrations can be tackled by the designed controller; the caveat is that the aberrations at consecutive frames should be correlated, such that the spatial correction applied to the aberration at previous frames is, to a certain extent, applicable to the current frame. The dynamic aberration was simulated through use of a spinning disc coated with hair spray, and it was ensured that the disc spun slowly enough so as to verify the aforementioned condition. The quality of the correction was assessed quantitatively by computing the temporal means and variances of the (spatial) variances of the center-of-mass deviations of the Shack-Hartmann pattern, and qualitatively by observing the quality of the resulting images. Each set of measurements was taken for a full revolution of the disc, and pictures were recorded every 50 frames.

At the end of the section, a per-frame comparison between the variances attained for all considered amounts of modes will be presented.

9.1 Uncorrected dynamic aberration

To serve as a basis for comparison, the performance metrics and pictures for select frames are hereby shown for a full uncorrected revolution of the disc:
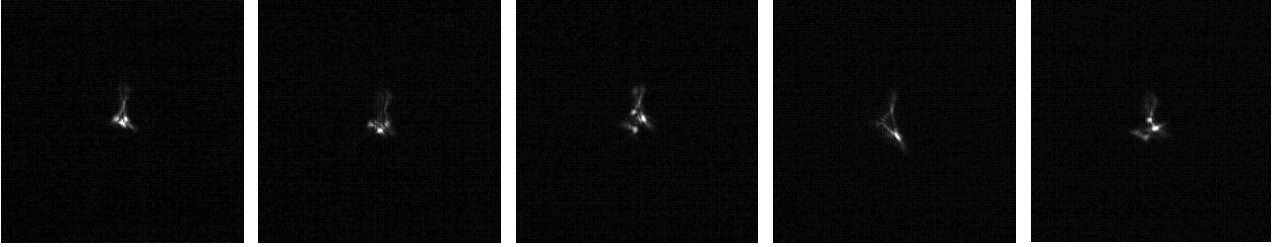

Figure 23: Select frames of the image resulting from the uncorrected dynamic aberration. From left to right: 50th frame; 250th frame; 450th frame; 600th frame; 950th frame

The mean of the spatial variances (of the center-of-mass displacements of the Shack-Hartmann pattern) along the full revolution was 1.85.

Although the pictures do not show this, as they were taken many frames apart, the aberration did not vary quickly between consecutive frames, so the controller is expected to improve the quality of the image over the whole revolution.
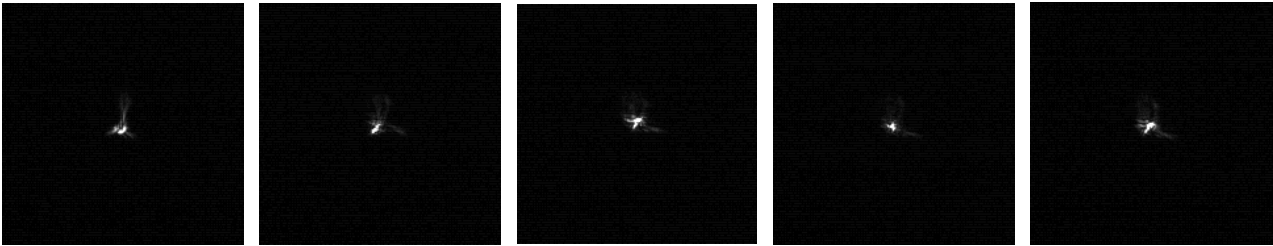
9.2 Dynamic aberration corrected with 40 modes

Figure 24: Select frames of the image resulting from the correction of the dynamic aberration with 40 modes. From left to right: 50th frame; 250th frame; 450th frame; 600th frame; 950th frame

The mean of the spatial variances along the full revolution was 1.08.

Figure 24 and the time mean of the spatial variances show successful improvement of the image quality.
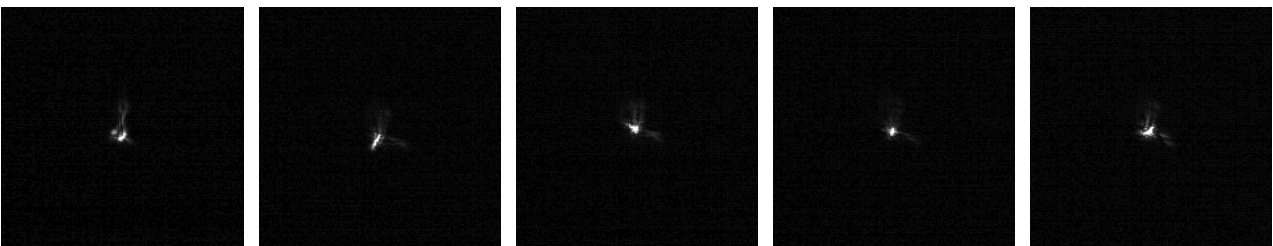
9.3 Dynamic aberration corrected with 38 modes

Figure 25: Select frames of the image resulting from the correction of the dynamic aberration with 40 modes. From left to right: 50th frame; 250th frame; 450th frame; 600th frame; 950th frame

The mean of the spatial variances along the full revolution was 1.06, suggesting somewhat of an improvement in image quality when compared to the 40-mode case. Figures 24 and 25 suggest that

the removal of the smallest two modes improved the correction of the aberration around the 450th frame, yet decreased the quality of correction of the aberration corresponding to the 50th frame.
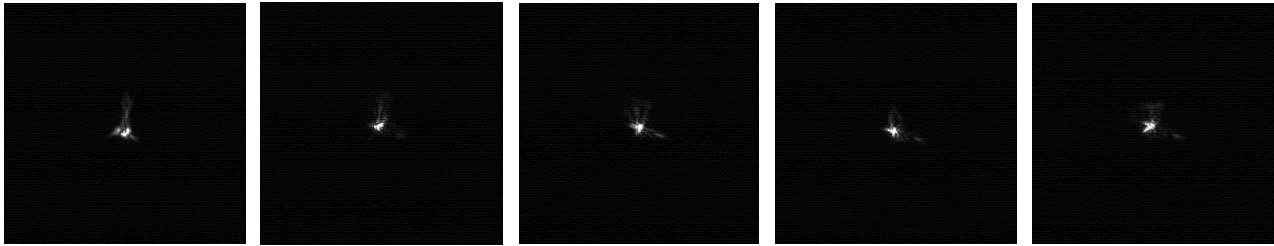
9.4 Dynamic aberration corrected with 30 modes

Figure 26: Select frames of the image resulting from the correction of the dynamic aberration with 30 modes. From left to right: 50th frame; 250th frame; 450th frame; 600th frame; 950th frame

The mean of the spatial variances saw an increase to 1.13, showing a drop in quality.
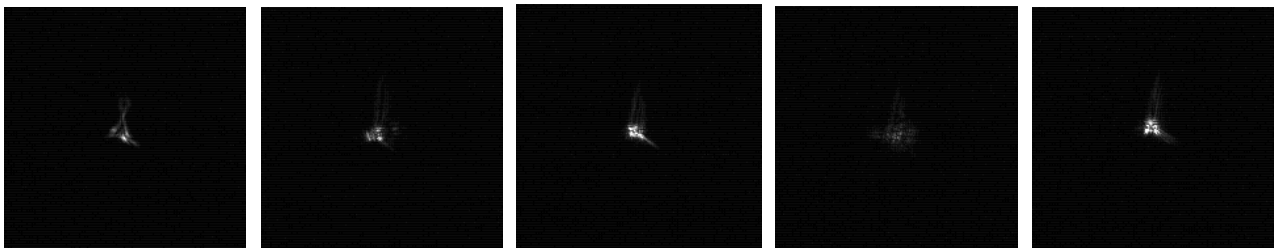
9.5 Dynamic aberration corrected with 5 modes

Figure 27: Select frames of the image resulting from the correction of the dynamic aberration with 5 modes. From left to right: 50th frame; 250th frame; 450th frame; 600th frame; 950th frame

Similarly to the previous subsection, correction with only five modes was unsuccessful. The mean of the spatial variances was 1.87, which is even slightly larger than the uncorrected value.
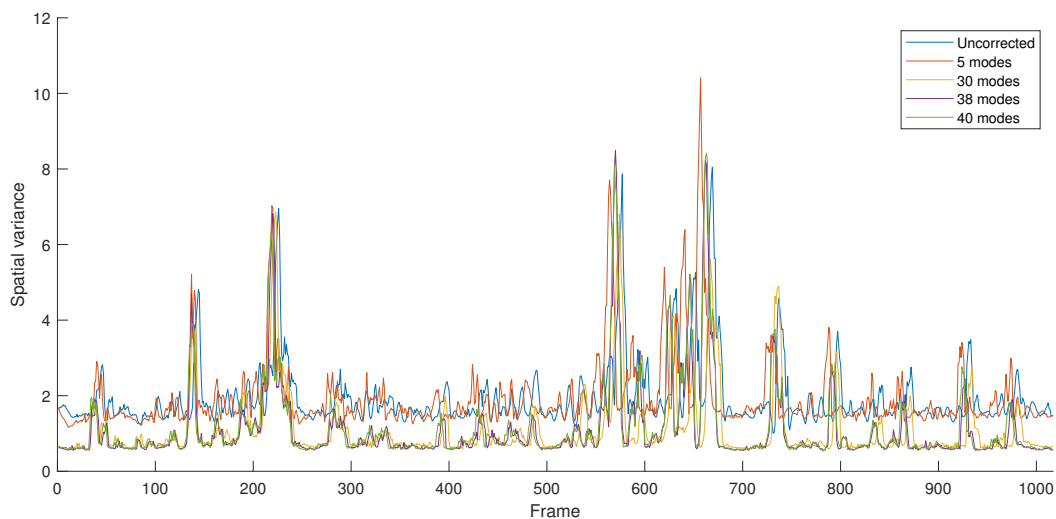
Spatial variance comparison

Figure 28: Comparison between the spatial variances per frame for the different amounts of modes

The variances obtained with 5-mode correction are on par with those of the uncorrected dynamic aberration, showing no improvement. Corrections with 30, 38, and 40 modes significantly improved the variances, warranting a dedicated comparison between them, as in Figure 29. Note that at the zones with the most aggressively varying aberrations (the sharp rises and drops around frames 180, 260, 615, and 700), the controller does not improve the image quality.
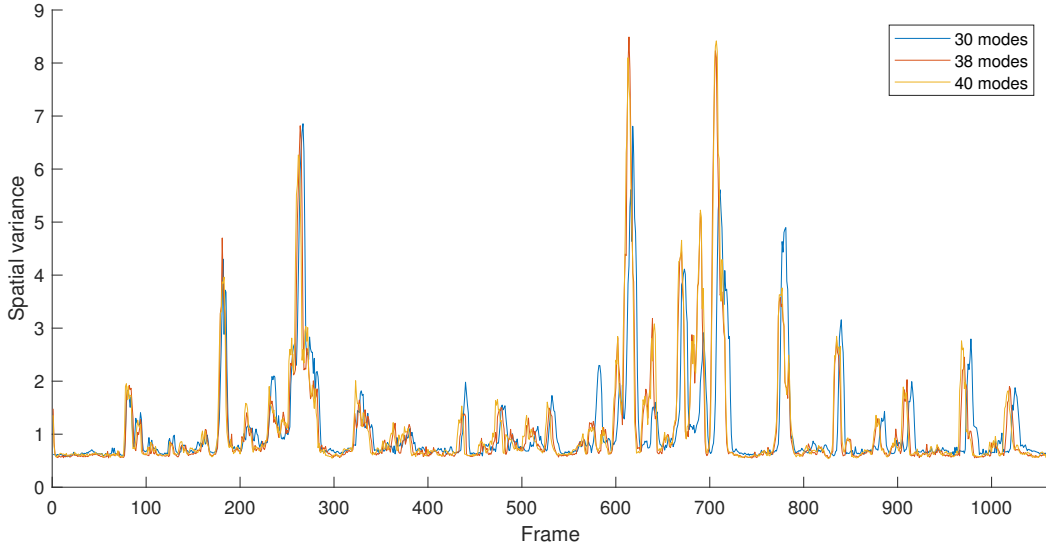

Figure 29: Comparison between the spatial variances per frame for correction done with 30, 38, and 40 modes

The correction with 30 modes tackled the less-aggressive aberrations worse than that done with larger amounts of modes. The corrections with 38 and 40 modes were the best, and very similar overall.

10   Conclusions

The experiments were successful, fulfilling, in general, the predictions made regarding the performance of the controller in the different scenarios, with both static and dynamic aberrations having been successfully tackled. Given that the control input is designed to spatially fit the wavefront at the current time and is then sent to the next time-step (as in Section 5), it was a challenge to create dynamic aberrations that were sufficiently correlated between consecutive frames, such that the controller successfully improved the image. Additionally, the amount of mirror actuators and their limitations meant that even static aberrations could give rise to problems, as aberrations of an order too high were impossible to correct. In light of these difficulties, many iterations of each scenario had to be done to ensure meaningful data was collected, leading to the satisfactory results obtained.

However, the truncation of the smallest singular values of H to compute its inverse was expected to improve the correction to some extent, but the results were inconsistent, with the amount of modes that performed better varying between scenarios due to uncertainties in the capture of H. The inevitable need to recompute the base voltages, reference, and H every once-so-often to account for hysteresis and changes in the environment also contributed to these inconsistencies, since, for example, the voltage reconstruction and the static aberration corrections were not done with the same base voltages or matrix H.

References

[1] Hamelinck. *Adaptive Deformable Mirror based on electromagnetic actuators* Technische Universiteit Eindhoven, 2010, Proefschrift (ISBN 978-90-386-2278-1)

[2] *https://www.thorlabs.com/newgrouppage9.cfm?objectgroup_id=5287*

[3] Verhaegen, Pozzi, Soloviev, Vdovin, Wilding. Stock, Mark W. Watson. *Control for High Resolution Imaging*